Cancer Research

Astrocyte Elevated Gene-1 Regulates Macrophage Activation in Hepatocellular Carcinogenesis

Chadia L. Robertson[1], Rachel G. Mendoza[1], Nidhi Jariwala[1], Mikhail Dozmorov[2,3], Nitai D. Mukhopadhyay[2,3], Mark A. Subler[1], Jolene J. Windle[1,3], Zhao Lai[4], Paul B. Fisher[1,3,5], Shobha Ghosh[6], and Devanand Sarkar[1,3,5]

Abstract

Chronic inflammation is a known hallmark of cancer and is central to the onset and progression of hepatocellular carcinoma (HCC). Hepatic macrophages play a critical role in the inflammatory process leading to HCC. The oncogene Astrocyte elevated gene-1 (*AEG-1*) regulates NFκB activation, and germline knockout of *AEG-1* in mice (AEG-$1^{-/-}$) results in resistance to inflammation and experimental HCC. In this study, we developed conditional hepatocyte- and myeloid cell–specific AEG-$1^{-/-}$ mice (AEG-$1^{\Delta HEP}$ and AEG-$1^{\Delta MAC}$, respectively) and induced HCC by treatment with N-nitrosodiethylamine (DEN) and phenobarbital (PB). AEG-$1^{\Delta HEP}$ mice exhibited a significant reduction in disease severity compared with control littermates, while AEG-$1^{\Delta MAC}$ mice were profoundly resistant. *In vitro*, AEG-$1^{-/-}$ hepatocytes exhibited increased sensitivity to stress and senescence. Notably, AEG-$1^{-/-}$ macrophages were resistant to either M1 or M2 differentiation with significant inhibition in migration, endothelial adhesion, and efferocytosis activity, indicating that AEG-1 ablation renders macrophages functionally anergic. These results unravel a central role of AEG-1 in regulating macrophage activation and indicate that AEG-1 is required in both tumor cells and tumor microenvironment to stimulate hepatocarcinogenesis.

Significance: These findings distinguish a novel role of macrophage-derived oncogene AEG-1 from hepatocellular AEG-1 in promoting inflammation and driving tumorigenesis.
Cancer Res; 78(22); 6436–46. ©2018 AACR.

Introduction

The risk factors for hepatocellular carcinoma (HCC) include viral hepatitis, alcoholism, and nonalcoholic fatty liver disease, all of which lead to chronic inflammation (1). Liver-resident macrophages (Kupffer cells) constitute approximately 20% of the total cells in the liver and play a vital role in establishing a proinflammatory, protumorigenic environment (2). During hepatocarcinogenesis, there is also infiltration of monocyte-derived macrophages into the liver further contributing to the inflammatory process. During initial tumorigenesis, damaged hepatocytes release cytokines, such as IL1β, which stimulate Kupffer cells to activate NFκB, resulting in the release of IL6 that activates the oncogenic STAT3 signaling in the hepatocytes thereby promoting proliferation of transformed cells (3–10). Concomitantly, tumor-associated macrophages (resident and infiltrating) also secrete various cytokines and chemokines, including IL1β, TNFα, IL6, CCL2, and CXCL10, which increase HCC cell proliferation and NFκB-mediated protection from HCC cell apoptosis, as well as angiogenic and growth factors, such as VEGF, PDGF, TGFβ, and FGF, which support HCC growth (2, 11). Understanding the mechanism of macrophage activation is, therefore, vital in controlling the chronic inflammatory process leading to HCC.

Our extensive studies over the last decade have firmly established that Astrocyte elevated gene-1 (*AEG-1*)/metadehrin (*MTDH*) functions as a major oncogene for HCC and is highly overexpressed in patients with HCC of diverse etiologies by multiple mechanisms including genomic amplification (12–22). *AEG-1* knockout mice (AEG-$1^{-/-}$) exhibit complete resistance to N-nitrosodiethylamine (DEN) and phenobarbital (PB)-induced HCC (20). Furthermore, AEG-1 ablation resulted in markedly reduced inflammation in mice because AEG-1 is fundamentally required for activation of NFκB, a key regulator of inflammatory process (20, 23–26). By directly interacting with p65 subunit of NFκB and CBP, AEG-1 functions as a bridging factor between NFκB and basal transcriptional machinery promoting NFκB-induced transcription (23, 24). Anchored on endoplasmic reticulum membrane, AEG-1 associates with upstream ubiquitinated activators of NFκB, such as RIP1 and TRAF2, facilitating their accumulation and subsequent NFκB activation (25). AEG-1 is directly phosphorylated by IKKβ, which is essential

[1]Department of Human and Molecular Genetics, Virginia Commonwealth University, Richmond, Virginia. [2]Department of Biostatistics, Virginia Commonwealth University, Richmond, Virginia. [3]Massey Cancer Center, Virginia Commonwealth University, Richmond, Virginia. [4]Greehey Children's Cancer Research Institute, University of Texas Health Science Center San Antonio, San Antonio, Texas. [5]VCU Institute of Molecular Medicine (VIMM), Virginia Commonwealth University, Richmond, Virginia. [6]Department of Internal Medicine, Virginia Commonwealth University, Richmond, Virginia.

Note: Supplementary data for this article are available at Cancer Research Online (http://cancerres.aacrjournals.org/).

Corresponding Author: Devanand Sarkar, Virginia Commonwealth University, School of Medicine, 1220 E Broad St, PO Box 980035, Richmond, VA 23298. Phone: 804-827-2339; Fax: 804-628-1176; E-mail: devanand.sarkar@vcuhealth.org

doi: 10.1158/0008-5472.CAN-18-0659

for IκBα degradation and NFκB activation (26). Indeed both AEG-1$^{-/-}$ hepatocytes and macrophages show inherent inability to activate NFκB upon lipopolysaccharide (LPS) treatment (20). Notably, AEG-1 itself is induced by inflammatory cytokines via NFκB thereby establishing a positive feedback between AEG-1 and NFκB (22, 27, 28).

Conversely, hepatocyte-specific AEG-1 transgenic mice (Alb/AEG-1) develop highly aggressive DEN-induced HCC compared with wild-type littermates, indicating a key regulatory role of AEG-1 in HCC cells (18, 19). AEG-1 expression in macrophages is markedly higher than that in hepatocytes (20). This observation coupled with the observations that AEG-1 is required for NFκB activation and inflammation suggest that AEG-1 might be important for regulating both tumor cells and tumor-associated macrophages. In this study, we interrogated the relative role of AEG-1 in these cells using tissue-specific conditional knockout mouse models. Our studies unravel a pivotal role of AEG-1 in regulating macrophage activation that profoundly affects HCC development.

Materials and Methods

Mice

All animal studies were approved by the Institutional Animal Care and Use Committee at Virginia Commonwealth University (Richmond, VA), and were performed in accordance with the Animal Welfare Act, the PHS Policy on Humane Care and Use of Laboratory Animals, and the U.S. Government Principles for the Utilization and Care of Vertebrate Animals Used in Testing, Research, and Training. Floxed AEG-1 mice (AEG-1$^{fl/fl}$) in C57BL/6 background (20) were crossed with Alb/Cre [B6.Cg-Tg (Alb-cre)21Mgn/J; ref. 29] and LysM/Cre (B6.129P2-*Lyz2*$^{tm1(cre)Ifo}$/J; Jackson Laboratories) mice (30) to generate AEG-1$^{\Delta HEP}$ (22) and AEG-1$^{\Delta MAC}$ mice, respectively. For induction of chemical carcinogenesis, a single intraperitoneal injection of 10 μg/gm body weight of DEN was given at 14 days of age to male mice and then PB (0.05%) was given daily in drinking water (20). The animals were sacrificed at 32 weeks of age. At the end of the experiment, liver, internal organs, and blood were collected. Serum liver enzymes were analyzed in the VCU Molecular Diagnostic Laboratory, Department of Pathology using standard procedures. For short-term DEN treatment, 2-week-old male mice were injected intraperitoneally with DEN (10 μg/gm). Apoptosis was determined by ApoAlert DNA Fragmentation Assay Kit (Takara) according to the manufacturer's protocol. For proliferation, mice were injected intraperitoneally with BrdU (100 μg/gm; Sigma) 2 hours before sacrifice and liver sections were stained using BrdU *In Situ* Detection Kit (BD Biosciences) according to the manufacturer's protocol.

Primary cells' isolation and culture conditions

All primary cells were used immediately after isolation in house and were *Mycoplasma* free as detected by Mycoplasma Detection Kit (Thermo Fisher Scientific). Primary mouse hepatocytes were isolated and cultured in Williams E Medium containing $NaHCO_3$, L-glutamine, insulin (1.5 mmol/L), and dexamethasone (0.1 mmol/L) as described previously (31). Kupffer cells were isolated from liver homogenates by centrifuging at 500 rpm for 10 minutes (32). The supernatant containing immune cells was sorted for CD11b$^+$F4/80$^+$ cells using BD FACSAria II (BD Biosciences). Bone marrow–derived macrophages (BMDM) and peritoneal macrophages were isolated according to standard protocols (33). Bone marrow cells were isolated from femurs of mice and were differentiated into macrophages using RPMI1640 medium supplemented with 10% heat-inactivated FBS and 100 U/mL recombinant mouse M-CSF for 7 days. At day 7, the media were changed to complete RPMI1640 containing 10% heat-inactivated FBS. For isolating primary peritoneal macrophages, mice were injected intraperitoneally with 4% thioglycollate and 4 days later macrophages were harvested in PBS via intraperitoneal injection. Macrophages were cultured in complete media for at least 12 hours prior to using for experiments. Liver sinusoidal endothelial cells (LSEC) were purified as described using short-term selective adherence and the purity was confirmed by staining with anti–Stabilin-2 antibody (Supplementary Fig. S1; ref. 34). All primary cells were isolated from male mice of 6–12 weeks of age, were cultured at 37°C and in 5% CO_2 with 100% humidity, and were used for experiments at 60%–80% confluence. BMDMs were treated with LPS (10 ng/mL) or IL4 (20 U/mL) for 7 hours.

Generation of Dihxy-sgAEG-1 cells

Dihxy cells, developed from DEN-injected C57BL/6 mice, were generously provided by Dr. Michael Karin's laboratory and cultured as described previously (6). The cells were *Mycoplasma* free as detected by Mycoplasma Detection Kit (Thermo Fisher Scientific) and were not used for more than 10 passages. These cells were transfected with a plasmid expressing either control, scrambled sgRNA or AEG-1 sgRNA, Cas9, puromycin-resistant marker, and mCherry (obtained from GeneCopoeia). Single clones from FACS-sorted mCherry-positive cells were isolated, expanded, and validated for *AEG-1* knockout.

Cell proliferation assays

Hepatocytes (1×10^4) were plated in each well of a 96-well plate for measuring proliferation by a standard MTT assay (35). For hypoxia assays, hepatocytes were cultured in 1% O_2 concentration in a hypoxic chamber (Ruskinn InVivo2 400, The Baker Company).

Efferocytosis assay

Efferocytosis was measured using Vybrant Phagocytosis Assay Kit (Thermo Fisher Scientific) according to the manufacturer's protocol.

Chemotaxis and migration assay

Migration of macrophages toward HCC cells was performed by a modified Boyden chamber assay in which macrophages were plated on the top chamber and HCC cells were plated on the bottom chamber and the macrophages were allowed to migrate for 24 hours. Migrated cells were fixed, stained with Giemsa, and counted.

LSEC adhesion assay

LSECs (5×10^5) were plated in each well of an 8-chamber slide and next day macrophages (5×10^3) were plated on top of LSEC monolayer for 30 minutes, following which, the nonadherent cells were washed with PBS, fixed, and stained using F4/80 antibody. The slides were mounted using a mounting medium containing DAPI (Vector Laboratories). The images were analyzed using an Olympus microscope capturing fluorescent and bright-field images.

Total RNA extraction, cDNA preparation, and real-time PCR

Total RNA was extracted from hepatocytes, macrophages, or mouse tissues using the Qiagen miRNAeasy Mini Kit (Qiagen). cDNA preparation was done using ABI cDNA Synthesis Kit (Applied Biosystems). Real-time PCR (RT-PCR) was performed using an ABI ViiA7 fast real-time PCR system and TaqMan gene expression assays according to the manufacturer's protocol (Applied Biosystems).

RNA sequencing

Total RNA, extracted using Qiagen miRNAeasy Mini Kit (Qiagen) from BMDMs of 3 adult mice per group, was employed for RNA sequencing. RNA-Seq library was prepared using Illumina TruSeq RNA sample preparation Kit and sequenced on Illumina HiSeq3000 platform. RNA-Seq libraries were pooled together to aim about 25–40M read passed filtered reads per sample. All sequencing reads were quality controlled using FastQC v0.11.2. Illumina adapters were trimmed using Cutadapt v1.9.dev2, replicates were merged and aligned with their reference genome (UCSC mouse genome build mm10) using subread-align v1.4.6-p4. The BAM files from alignment were processed using featureCounts v1.4.6-p4 to obtain the counts per gene in all samples. Mus_musculus.GRCm38.83.gtf gene definition file was used. The differential expression analysis was performed using edgeR v3.18.1. Genes having counts per million less than two in all samples were excluded. Differentially expressed genes were defined using $P< 0.01$ and FDR-corrected $P < 0.1$ cutoffs. All bioinformatics analyses were conducted in R/Bioconductor computing environment v3.4.0. GEO Series accession number of this dataset is GSE107691.

Western blotting analysis

Cell lysates and tissue extracts were prepared and Western blotting was performed as described previously (20). The primary antibodies used were anti-AEG-1 (chicken, inhouse, 1:5,000), ATM (Santa Cruz Biotechnology, mouse monoclonal, 1:500), phospho-ATM (Cell Signaling Technology, rabbit polyclonal, 1:1,000), ATR (Cell Signaling Technology, rabbit polyclonal, 1:1,000), phospho-ATR (Cell Signaling Technology, rabbit polyclonal, 1:1,000), CHK1 (Santa Cruz Biotechnology, mouse monoclonal, 1:200), phospho-CHK1 (Cell Signaling Technology, rabbit polyclonal, 1:1,000), CHK2 (Santa Cruz Biotechnology, mouse monoclonal, 1:200), phospho-CHK2 (Cell Signaling Technology, rabbit polyclonal, 1:1,000), p53 (Cell Signaling Technology, mouse monoclonal, 1:1,000), phospho-p53 (Cell Signaling Technology, mouse monoclonal, 1:1,000), p21 (Cell Signaling Technology, rabbit polyclonal, 1:1,000), and anti-GAPDH (Santa Cruz Biotechnology, mouse monoclonal, 1:1,000 and Cell Signaling Technology, rabbit polyclonal, 1:1,000). Densitometric analysis was performed using ImageJ software (NIH, Bethesda, MD).

IHC and immunofluorescence assays

IHC was performed on formalin-fixed paraffin-embedded (FFPE) sections as described previously (20) using anti-AEG-1 (chicken, in-house) and anti-PCNA (Cell Signaling Technology #13110) antibodies. Immunofluorescence was performed on FFPE sections using anti-AEG-1 (chicken, in-house) and F4/80 (AbD Serotec #MCA497RT) antibodies. Hepatocytes were cultured in collagen-1–coated 4-chamber slides and immunofluorescence was performed using antibody against γH2AX (Cell Signaling Technology #5438). LSECs were cultured in 8-chamber slides and immunofluorescence was performed using anti–Stabilin-2 antibody (MBL International #D317-3). For IHC, images were analyzed using an Olympus microscope. For immunofluorescence, images were analyzed using a Zeiss confocal laser scanning microscope.

Senescence-associated β-galactosidase assay

Hepatocytes were cultured for 3 days and senescence-associated β-galactosidase (SA-β-Gal) activity was measured as described previously (35).

Bayesian statistical analysis

Bayesian analysis (19) was performed to analyze the effect of hepatocyte- and macrophage-specific deletion of AEG-1 on hepatocarcinogenesis in mice. All analysis was done using the statistical computing software R v 3.3.2. The experiment measured effects of different gene mutation on liver health through a resulting tumor counts of various sizes. The notation for the responses were:

NT = number of tumors.
X1 = number of tumors of size <1 mm.
X2 = number of tumors of size 1–2 mm.
X3 = number of tumors of size 3–5 mm.
X4 = number of tumors of size 6-8 mm.
X5 = number of tumors of size above 20 mm.

In certain cases, the whole liver was reported to be tumor. In that case, the response for each type of tumor size was taken to be the maximum value among all animals of that type of tumor. The covariates or the independent variables of the experiment were type of gene mutation. The statistical model needed to accommodate a regression for counts as well as multinomial response regression. We implemented this in a Bayesian model with Poisson regression for tumor count and Multinomial regression for the observed proportion of the tumors in the five categories. In the notations used above, the statistical model is:

$$N_T \sim \text{Poi}(\lambda)$$
$$\log(\lambda) \sim N(\beta_0 + \beta_{HEP}(\Delta HEP) + \beta_{MAC}(\Delta MAC), \sigma_2{}^2)$$
$$(X_1, X_2, X_3, X_4, X_5) \mid N_T \sim \text{Multinomial}(\pi_1, \pi_2, \pi_3, \pi_4, \pi_5)$$

The structure above was implemented using a Bayesian model. All the unrestricted parameters were given flat noninformative normal prior centered at zero and variance 10^6. Posterior distribution was computed using Markov chain Montecarlo simulation with initial burn in 20,000 samples. Convergence of the model was assured using Brooks–Gelman–Rubin diagnostics. We observed multivariate PSRF = 1.05 and the PSRF for individual parameters was less than 1.1. A sample of 8,000, thinned by three was used to estimate the parameters of the model.

We report, instead of the estimated parameter values, the predicted values for number of tumors in each type of mice and distribution of the tumors into size categories. All estimates were obtained from the posterior distribution of the model after convergence. The summary of the MCMC outputs are shown in Supplementary Tables S1–S4.

Statistical analysis

Data were represented as the mean ± SEM and analyzed for statistical significance using one-way ANOVA followed by Newman–Keuls test as a *post hoc* test.

Results

Our previous studies demonstrated profound resistance to DEN/PB-induced HCC in AEG-$1^{-/-}$ mice (20). Inflammation is an integral component of DEN-induced HCC and we documented that activation of NFκB, a key regulator of inflammation, was markedly abrogated in AEG-$1^{-/-}$ hepatocytes and macrophages compared with AEG-$1^{+/+}$ (20). In DEN-treated AEG-$1^{+/+}$ livers, colocalization studies using anti-AEG-1 and F4/80 antibodies revealed increased AEG-1 in macrophages compared with hepatocytes (Fig. 1A; Supplementary Fig. S2A). In DEN-treated AEG-$1^{-/-}$ livers, which did not show induction of HCC, F4/80-positive macrophages were sparse, compared with DEN-treated AEG-$1^{+/+}$ livers (Fig. 1A; Supplementary Fig. S2A). In naïve adult wild-type liver, higher AEG-1 staining was observed in F4/80-positive macrophages compared with hepatocytes (Supplementary Fig. S2B) and AEG-1 mRNA levels in isolated Kupffer cells were approximately 4 times higher compared with isolated hepatocytes (Supplementary Fig. S2C). These findings indicate that AEG-1 might play a regulatory role in macrophage activation during DEN-induced HCC.

To interrogate the role of hepatocyte and macrophage AEG-1 in HCC, we created hepatocyte- and myeloid cell–specific conditional AEG-$1^{-/-}$ mice (AEG-$1^{\Delta HEP}$ and AEG-$1^{\Delta MAC}$, respectively), by crossing AEG-$1^{fl/fl}$ mice with Alb/Cre (29) and LysM/Cre (30) mice, respectively. We have described authenticity of AEG-$1^{\Delta HEP}$ mice previously (22). AEG-$1^{\Delta HEP}$ mice were used to study the role of AEG-1 in nonalcoholic steatohepatitis but the response of AEG-$1^{\Delta HEP}$ mice to HCC development has not been studied. We now demonstrate Kupffer cell–specific AEG-1 knockout in AEG-$1^{\Delta MAC}$ mice by TaqMan-qRT-PCR, Western blot, and IHC analyses (Fig. 1B–D). AEG-1 expression was lost from F4/80-positive Kupffer cells in AEG-$1^{\Delta MAC}$ mice (Fig. 1D).

HCC was induced by DEN/PB treatment in AEG-$1^{fl/fl}$, AEG-$1^{\Delta HEP}$, and AEG-$1^{\Delta MAC}$ littermates. Control AEG-$1^{fl/fl}$ littermates, obtained by mating with either Alb/Cre or LysM/Cre mice, showed similar phenotypes and therefore the findings from all AEG-$1^{fl/fl}$ mice were clustered together. Upon treatment with DEN/PB, at 32 weeks, AEG-$1^{fl/fl}$ mice developed robust multinodular HCC, AEG-$1^{\Delta HEP}$ developed HCC of significantly less magnitude than AEG-$1^{fl/fl}$ mice, while AEG-$1^{\Delta MAC}$ mice were profoundly resistant (Fig. 2A and B; Table 1). Liver weight of AEG-$1^{fl/fl}$ mice was significantly higher than that of AEG-$1^{\Delta HEP}$ and AEG-$1^{\Delta MAC}$ mice and liver weight of AEG-$1^{\Delta HEP}$ mice was significantly higher than that of AEG-$1^{\Delta MAC}$ mice as a reflection of total tumor load (Fig. 2C). To obtain additional significance, we performed Bayesian statistical analysis to check the probability of tumorigenesis using number and size of the nodules as the response variables (Fig. 2D). The probability of no tumor formation was profoundly low in AEG-$1^{fl/fl}$ mice compared with the other two groups (Fig. 2D).

Hemotoxylin and eosin staining of liver sections showed HCC with loss of hepatic architecture in AEG-$1^{fl/fl}$ mice, while in AEG-$1^{\Delta HEP}$ and AEG-$1^{\Delta MAC}$ mice liver architecture was

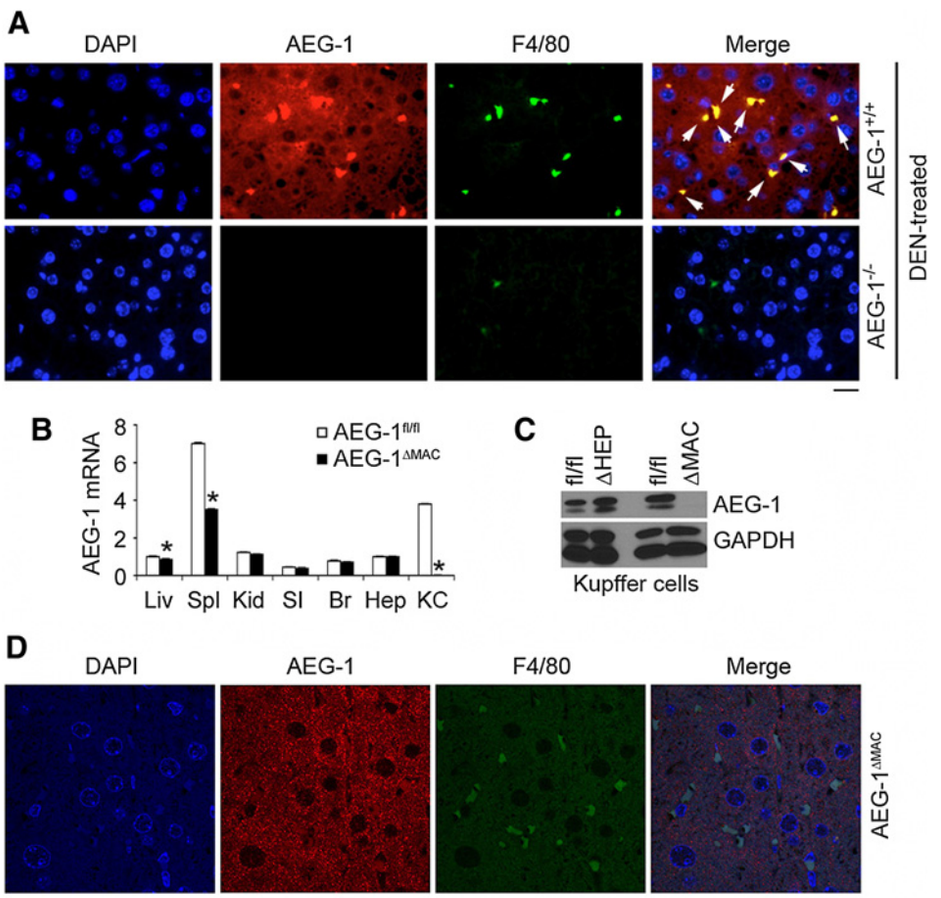

Figure 1.

Macrophages express AEG-1. **A,** Representative images of FFPE liver sections from DEN-treated AEG-$1^{+/+}$ and AEG-$1^{-/-}$ mice stained with anti-AEG-1 (red) and F4/80 (green) antibodies. Yellow in merged panels indicates localization of AEG-1 in macrophages (arrows). Magnification, ×400. Scale bar, 20 μm. **B–D,** Analysis of AEG-1 expression in AEG-$1^{fl/fl}$ and AEG-$1^{\Delta MAC}$ mice by TaqMan qRT-PCR (**B**), Western blot analysis (**C**), and IHC with anti-AEG-1 (red) and F4/80 (green) antibodies (**D**). For **B**, data were normalized by GAPDH levels. Data represent mean ± SEM. *, $P < 0.01$ versus AEG-$1^{fl/fl}$. Liv, liver; Spl, spleen; Kid, kidney; SI, small intestine; Br, brain; Hep, hepatocytes; KC, Kupffer cells.

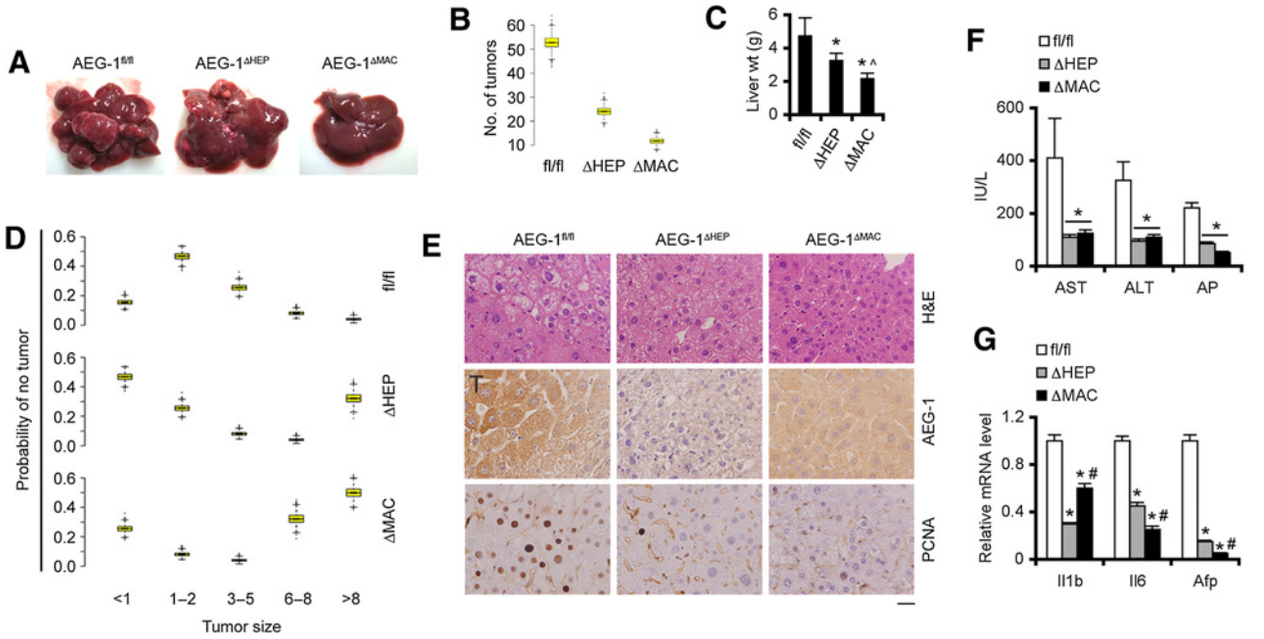

Figure 2.

AEG-1$^{\Delta HEP}$ and AEG-1$^{\Delta MAC}$ mice are resistant to experimental HCC. AEG-1$^{fl/fl}$, AEG-1$^{\Delta HEP}$, and AEG-1$^{\Delta MAC}$ mice (7 per group) received an initial DEN injection, followed by PB treatment in drinking water. The mice were sacrificed at 32 weeks when all data points were analyzed. **A,** Representative photographs of the livers. **B,** Total number of tumors. **C,** Liver weight of the mice. Data represent mean ± SEM. *, $P < 0.01$ versus fl/fl; ^, $P < 0.01$ versus ΔHEP. **D,** Bayesian analysis demonstrating probability of no tumor. **E,** Top, hematoxylin and eosin staining of liver sections; middle and bottom, AEG-1 and PCNA staining of the liver sections, respectively. Magnification, ×400. Scale bar, 20 μm. T, tumor. **F,** Serum levels of the indicated liver enzymes. AST, aspartate aminotransferase; ALT, alanine aminotransferase; and AP, alkaline phosphatase. **G,** Relative mRNA levels of the indicated genes. GAPDH levels were used for normalization. For **F** and **G**, data represent mean ± SEM. *, $P < 0.01$ versus fl/fl; #, $P < 0.01$ versus ΔHEP.

relatively well preserved (Fig. 2E, top; Supplementary Fig. S3). IHC staining for AEG-1 in liver sections revealed intense staining in AEG-1$^{fl/fl}$ mice, especially in the tumor, no staining in AEG-1$^{\Delta HEP}$ mice, and homogenous staining in hepatocytes in AEG-1$^{\Delta MAC}$ mice (Fig. 2E, middle; Supplementary Fig. S3). IHC staining for PCNA, a marker for cell proliferation, showed a marked increase in PCNA-positive cells in AEG-1$^{fl/fl}$ livers compared with AEG-1$^{\Delta HEP}$ and AEG-1$^{\Delta MAC}$ livers (Fig. 2E, bottom). Levels of serum liver enzymes, aspartate aminotransferase (AST), alanine aminotransferase (ALT), and alkaline phosphatase (AP), were significantly higher in AEG-1$^{fl/fl}$ mice versus AEG-1$^{\Delta HEP}$ and AEG-1$^{\Delta MAC}$ mice indicative of liver damage (Fig. 2F). The levels of mRNA for α-fetoprotein, a specific marker for HCC, were robustly higher in the livers of AEG-1$^{fl/fl}$ mice compared with the other two groups (Fig. 2G). In DEN-induced tumorigenesis, damaged hepatocytes release cytokines, such as IL1β, which stimulate Kupffer cells to release IL6 (3–10). Both IL1β and IL6 mRNA levels were significantly higher in AEG-1$^{fl/fl}$ livers versus AEG-1$^{\Delta HEP}$ and AEG-1$^{\Delta MAC}$ livers (Fig. 2G). IL1β mRNA levels were higher in AEG-1$^{\Delta MAC}$ liver compared with AEG-1$^{\Delta HEP}$ liver, indicating that damaged hepatocytes in AEG-1$^{\Delta MAC}$ liver can still produce IL1β. IL6 mRNA levels were lower in AEG-1$^{\Delta MAC}$ liver compared with AEG-1$^{\Delta HEP}$ liver, indicating inhibition of macrophage activation in AEG-1$^{\Delta MAC}$ liver.

Similar to chronic liver disease, DEN treatment results in DNA damage and apoptosis in the hepatocytes (5, 36). This damage triggers compensatory proliferation and repair. Upon activation of survival pathways, the damaged (and mutated) hepatocytes escape apoptosis and proliferate, resulting in expansion of mutated, transformed cells. Induction of senescence in premalignant cells and clearing of these senescent cells by the immune system is a mechanism of HCC inhibition (37). When AEG-1$^{-/-}$ hepatocytes, isolated from AEG-1$^{\Delta HEP}$ mice, were deprived of growth

Table 1. Number and sizes of nodules in DEN/PB-treated mice at 32 weeks.

	No. of nodules (in mm)				
ID	<1	1–2	3–5	6–8	>8
fl/fl1	Entire liver				
fl/fl2	Entire liver				
fl/fl3	Entire liver				
fl/fl4	0	7	10	5	2
fl/fl5	0	18	1	4	2
fl/fl6	7	30	12	2	2
fl/fl7	0	25	17	1	0
ΔHEP1	10	5	3	0	0
ΔHEP2	6	2	0	0	0
ΔHEP3	4	29	10	4	0
ΔHEP4	15	9	2	0	0
ΔHEP5	0	17	0	0	0
ΔHEP6	8	0	4	0	0
ΔHEP7	11	22	6	1	0
ΔMAC1	5	0	0	0	0
ΔMAC2	2	0	0	0	0
ΔMAC3	8	4	0	0	0
ΔMAC4	3	11	1	0	0
ΔMAC5	10	0	4	0	0
ΔMAC6	16	5	2	0	0
ΔMAC7	5	6	0	0	0

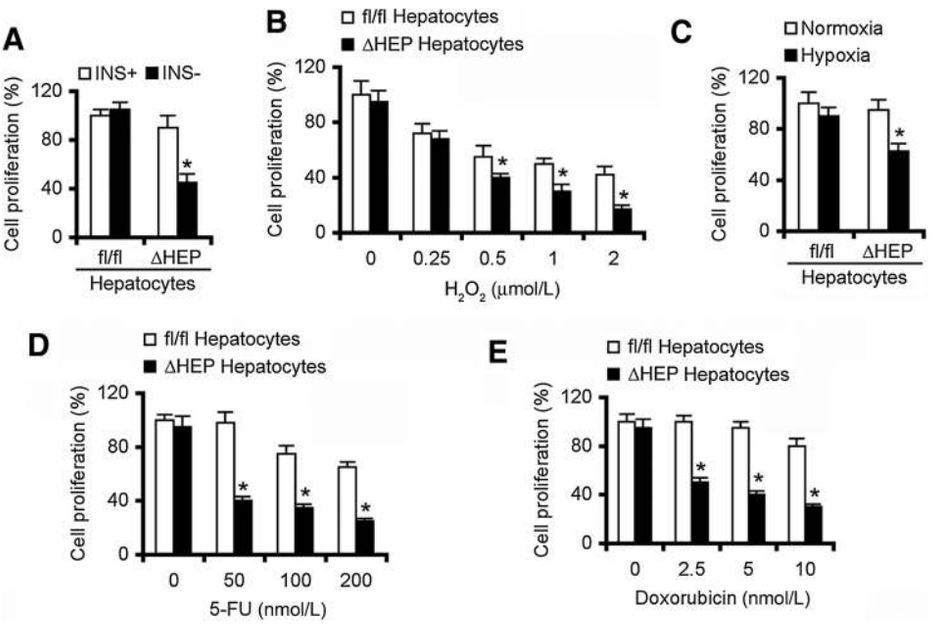

Figure 3.
AEG-$1^{-/-}$ hepatocytes are susceptible to stress. Proliferation of hepatocytes, isolated from AEG-$1^{fl/fl}$ and AEG-$1^{\Delta HEP}$ mice, was analyzed by MTT assay 48 hours after treatment that included insulin (INS) deprivation (**A**), H_2O_2 treatment at the indicated doses (**B**), hypoxia (**C**), 5-fluorouracil (5-FU) treatment at the indicated doses (**D**), and doxorubicin treatment at the indicated doses (**E**). Data represent mean ± SEM of triplicate experiments, each containing eight data points per group. *, $P < 0.01$ versus hepatocytes isolated from AEG-$1^{fl/fl}$ mice.

factor, such as insulin, or subjected to stressors including H_2O_2, hypoxia, and chemotherapeutic drugs, such as 5-fluorouracil (5-FU) and doxorubicin, they showed significantly increased susceptibility compared with AEG-$1^{+/+}$ hepatocytes, isolated from AEG-$1^{fl/fl}$ mice (Fig. 3A–E). In *in vitro* culture, mouse hepatocytes do not proliferate and enter senescence after 4 days of culture. At 3 days of culture AEG-$1^{-/-}$ hepatocytes, isolated from AEG-$1^{\Delta HEP}$ mice, showed marked induction of senescence, measured by SA-β-gal assay and senescent-associated heterochromatic foci assay, compared with AEG-$1^{+/+}$ hepatocytes, isolated from AEG-$1^{fl/fl}$ mice (Fig. 4A–C). *In vitro* treatment with DEN unraveled increased sensitivity of AEG-$1^{-/-}$ hepatocytes compared with AEG-$1^{+/+}$ (Fig. 4D). DEN treatment induced DNA damage response, indicated by activation of ATM and ATR, their downstream kinases CHK1 and CHK2 leading to p53 phosphorylation and increase in p53-target p21 levels in AEG-$1^{+/+}$ hepatocytes (Fig. 4E; Supplementary Fig. S4A). However, this response was markedly pronounced in AEG-$1^{-/-}$ hepatocytes (Fig. 4E; Supplementary Fig. S4A). DNA damage response following DEN treatment was similar in hepatocytes isolated from AEG-$1^{fl/fl}$ and AEG-$1^{\Delta MAC}$ mice (Supplementary Fig. S4B), indicating that it is the lack of AEG-1 in hepatocytes isolated from AEG-$1^{\Delta HEP}$ mice that confers increased susceptibility to DEN. These notions were confirmed further by *in vivo* assays, in which short-term DEN treatment resulted in increased apoptosis and decreased compensatory proliferation in AEG-$1^{\Delta HEP}$ livers when compared with AEG-$1^{fl/fl}$ and AEG-$1^{\Delta MAC}$ livers (Fig. 4F). Collectively, these findings indicate that AEG-$1^{-/-}$ hepatocytes are more susceptible to stress and are prosenescent so that these hepatocytes may not sustain survival and proliferation to promote the tumorigenic process thereby explaining dampened hepatocarcinogenic response in AEG-$1^{\Delta HEP}$ mice.

To understand how AEG-1 regulates macrophages so that AEG-$1^{\Delta MAC}$ mice become resistant to DEN/PB-induced HCC, we analyzed differential gene expression profiles in naïve BMDMs isolated from AEG-$1^{fl/fl}$ and AEG-$1^{\Delta MAC}$ mice, by RNA-Seq. Using a FDR < 0.01 and $P < 0.01$, 1,104 genes showed upregulation and 1,011 genes showed downregulation in AEG-$1^{-/-}$ BMDMs compared with AEG-$1^{+/+}$ (Fig. 5A). Differentially changed genes were analyzed using Ingenuity pathway analysis software to identify the upstream regulators the activation or inhibition of which might lead to alterations in downstream genes. A *z*-score > 2 indicates activation and a score of ≤2 indicates inhibition. A highly significant ($P < 10^{-7}$) and robust inhibition of upstream regulators of inflammation, immune response, and cytokine signaling, such as LPS, IFNγ, TNFα, IL5, IL2, IL4, IL15, and IL3, toll-like receptor 4 (TLR4), lymphotoxin α (TNFSF1), myeloid differentiation primary response 88 (MYD88), inhibitor of nuclear factor kappa B kinase subunit beta (IKBKB), TGFβ1, and CpG oligonucleotides, was observed in AEG-$1^{-/-}$ BMDMs compared with AEG-$1^{+/+}$ (Fig. 5B). In addition, growth-regulatory molecules such as c-Myc and VEGF (VEGFA) were also inhibited in AEG-$1^{-/-}$ BMDMs, suggesting that knocking out AEG-1 results in profound inhibition in macrophage function.

Tumor development is associated with a switch in macrophage phenotype from M1 (classically activated state), which is associated with a proinflammatory response, to M2 (alternatively activated), which promotes angiogenesis and tissue remodeling as well as immunosuppression (38–40). In HCC, M1 macrophages are required for the initiation of HCC while M2 macrophages are required for the sustenance of the disease. As a chronic inflammatory disease, HCC livers show a flux of M1 and M2 macrophages. We treated AEG-$1^{+/+}$ and AEG-$1^{-/-}$ BMDMs, isolated from AEG-$1^{fl/fl}$ and AEG-$1^{\Delta MAC}$ mice, respectively, with LPS that induces M1 differentiation. A robust increase in the mRNA levels of Il12, Il6, and iNos, markers of M1 activation, was observed in LPS-treated AEG-$1^{+/+}$ BMDMs but not AEG-$1^{-/-}$ BMDMs (Fig. 5C). Similarly, IL4 treatment to induce M2 differentiation failed to augment Il10 and Arg1, markers of M2 activation, in AEG-$1^{-/-}$ BMDMs (Fig. 5D).

To dissect the interplay of AEG-1 in HCC cells and macrophages, we knocked out AEG-1 by CRISPR/Cas9 in mouse HCC cells Dihxy (Fig. 6A; ref. 6). AEG-1–null Dihxy cells (Dihxy-sgAEG-1) exhibited marked decreases in proliferation compared

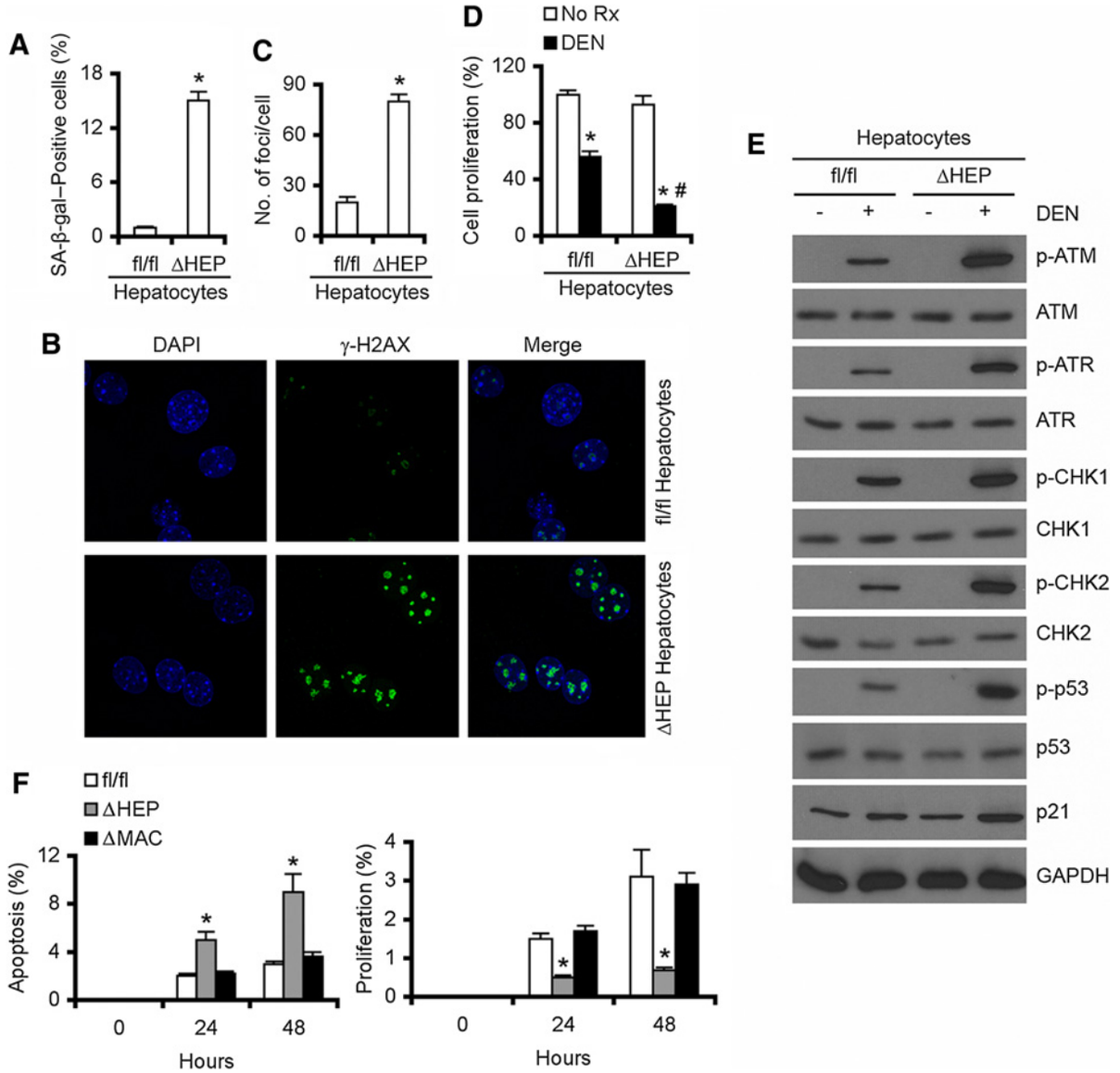

Figure 4.

AEG-1$^{-/-}$ hepatocytes are prosenescent and susceptible to DEN-induced DNA damage. AEG-1$^{+/+}$ and AEG-1$^{-/-}$ hepatocytes, isolated from AEG-1$^{fl/fl}$ and AEG-1$^{\Delta HEP}$ mice, respectively, were cultured for 3 days and senescence was determined by senescence-associated SA-β-Gal assay (**A**) and immunofluorescence staining for γH2AX (**B** and **C**). For **B**, magnification, ×630. **D,** Proliferation of AEG-1$^{+/+}$ and AEG-1$^{-/-}$ hepatocytes, isolated from AEG-1$^{fl/fl}$ and AEG-1$^{\Delta HEP}$ mice, respectively, was analyzed by MTT assay 48 hours after DEN (25 ng/mL) treatment. **E,** Western blot analysis for the indicated proteins in AEG-1$^{+/+}$ and AEG-1$^{-/-}$ hepatocytes, isolated from AEG-1$^{fl/fl}$ and AEG-1$^{\Delta HEP}$ mice, respectively, treated or not with DEN (25 ng/mL) for 8 hours. GAPDH was used as loading control and one representative image for GAPDH levels is shown. **F,** AEG-1$^{fl/fl}$, AEG-1$^{\Delta HEP}$, and AEG-1$^{\Delta MAC}$ mice were treated with DEN (10 μg/g) and apoptosis was determined by TUNEL assay (left) and proliferation was determined by BrdU incorporation assay (right). For **A** and **C**, data represent mean ± SEM. *, $P < 0.01$ versus hepatocytes isolated from AEG-1$^{fl/fl}$ mice. For **D**, data represent mean ± SEM. *, $P < 0.01$ versus corresponding No Rx; #, $P < 0.01$ versus hepatocytes isolated from AEG-1$^{fl/fl}$ mice. For **F**, data represent mean ± SEM. *, $P < 0.01$ versus AEG-1$^{fl/fl}$ and AEG-1$^{\Delta MAC}$.

with parental Dihxy cells and Dihxy cells expressing control, scrambled sgRNA (Dihxy-sgCon; Fig. 6B). We treated AEG-1$^{+/+}$ and AEG-1$^{-/-}$ BMDM, isolated from AEG-1$^{fl/fl}$ and AEG-1$^{\Delta MAC}$ mice, respectively, with conditioned medium (CM) from Dihxy-sgCon and Dihxy-sgAEG-1 cells and measured mRNA levels of M1 markers Il12, Il6, and iNos, and M2 markers Il10 and Arg1 (Fig. 6C). Upon treatment with CM from Dihxy-sgCon cells, AEG-1$^{+/+}$ BMDMs showed more robust induction of M2 markers Il10 and Arg1 than M1 markers, indicating that HCC cells direct wild-type macrophages toward M2 differentiation. The induction of M1 and M2 markers were significantly decreased when AEG-1$^{+/+}$ BMDM were treated with CM from Dihxy-sgAEG-1 cells. AEG-1$^{-/-}$ BMDMs showed little to no induction of the M1 and M2 markers upon treatment with CM from either

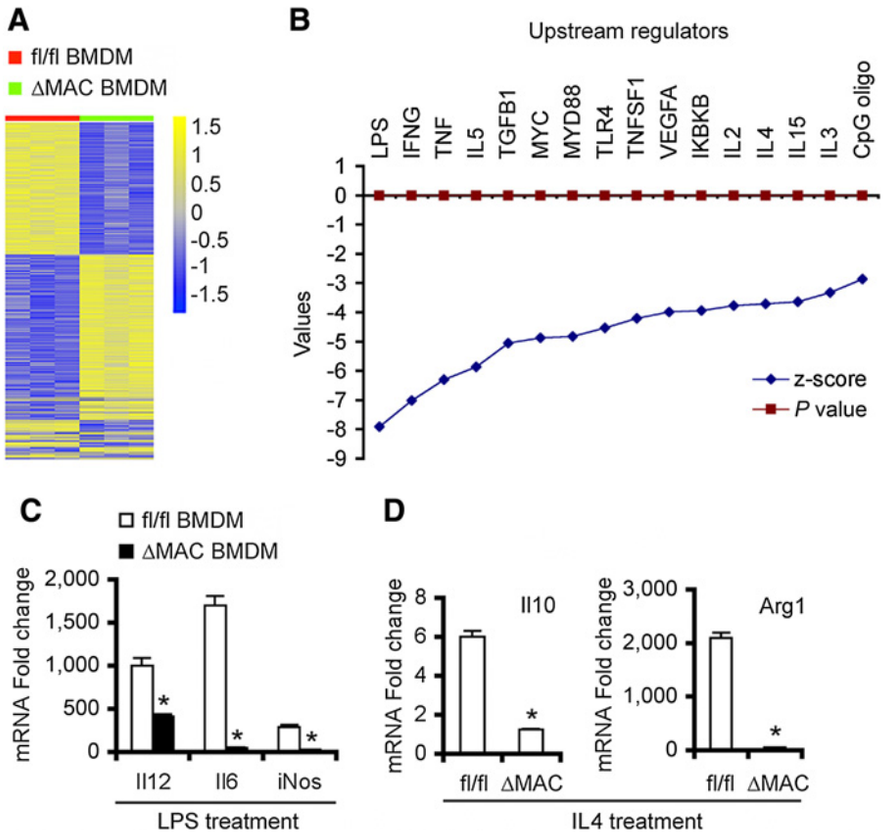

Figure 5.
AEG-1$^{-/-}$ macrophages resist M1 or M2 differentiation. **A,** Heatmap of differentially expressed genes in AEG-1$^{+/+}$ and AEG-1$^{-/-}$ BMDMs, isolated from AEG-1$^{fl/fl}$ and AEG-1$^{\Delta MAC}$ mice, respectively. **B,** Upstream regulators inhibited in AEG-1$^{-/-}$ BMDM. $P < 10^{-7}$ thus approaching 0 in the graph. **C** and **D,** BMDMs, isolated from AEG-1$^{fl/fl}$ and AEG-1$^{\Delta MAC}$ mice, were treated with 10 ng/mL LPS (**C**) or 20 U/mL IL4 (**D**) for 7 hours and the levels of the indicated mRNAs were measured by TaqMan qRT-PCR. Data represent mRNA fold change over untreated samples and were normalized by GAPDH levels. Data represent mean ± SEM of triplicate experiments. *, $P < 0.01$ versus BMDMs isolated from AEG-1$^{fl/fl}$ mice.

Dihxy-sgCon or Dihxy-sgAEG-1 cells. Collectively, these findings indicate that lack of AEG-1 renders the macrophages anergic so that they are unable to respond to any stimuli.

We next analyzed migration of AEG-1$^{+/+}$ and AEG-1$^{-/-}$ BMDMs, isolated from AEG-1$^{fl/fl}$ and AEG-1$^{\Delta MAC}$ mice, respectively, employing a Boyden chamber assay wherein BMDMs were plated on the top chamber and Dihxy-sgCon or Dihxy-sgAEG-1 cells were plated on the bottom chamber. Migration of AEG-1$^{+/+}$ BMDMs toward Dihxy-sgCon cells were significantly higher than that of AEG-1$^{-/-}$ BMDMs (Fig. 6D). In addition, migration of AEG-1$^{+/+}$ BMDMs toward Dihxy-sgAEG-1 cells was significantly lower than that toward Dihxy-sgCon cells, an effect further decreased in AEG-1$^{-/-}$ BMDMs (Fig. 6D). These observations were confirmed in an *in vivo* system in which AEG-1$^{+/+}$ and total AEG-1$^{-/-}$ mice were injected with DEN at 2 weeks and transformed hepatocytes and BMDMs were isolated at 12 weeks. AEG-1$^{+/+}$ and AEG-1$^{-/-}$ BMDMs were treated with CM from AEG-1$^{+/+}$ and AEG-1$^{-/-}$ hepatocytes and subjected to assays for M1 and M2 markers and migration (Fig. 6E and F). Activation of M1 and M2 markers and migration of AEG-1$^{-/-}$ BMDMs were significantly less compared with AEG-1$^{+/+}$ BMDMs treated with CM from AEG-1$^{+/+}$ and AEG-1$^{-/-}$ hepatocytes. NFκB-regulated cytokines and chemokines, released from Dihxy-sgCon cells and AEG-1$^{+/+}$ hepatocytes, stimulate migration of macrophages. AEG-1 is fundamentally required for NFκB activation and in Dihxy-sgAEG-1 cells and AEG-1$^{-/-}$ hepatocytes deficiency of NFκB-regulated cytokines and chemokines might decrease migration of AEG-1$^{-/-}$ macrophages. Efferocytosis is a functional activity of macrophages, which was markedly inhibited in AEG-1$^{-/-}$ macrophages compared with AEG-1$^{+/+}$ further documenting functional anergy (Fig. 6G).

Kupffer cells reside on LSECs (2). Macrophages interact with endothelial cells by means of selectin P-ligand, integrins, and other cell adhesion molecules (41). Many of these genes are downstream of NFκB and our previous study documented upregulation of these genes by AEG-1 (23). We thus hypothesize that knocking down AEG-1 might interfere with adhesion of macrophages to endothelial cells. AEG-1$^{+/+}$ and AEG-1$^{-/-}$ Kupffer cells, isolated from AEG-1$^{fl/fl}$ and AEG-1$^{\Delta MAC}$ mice, respectively, were plated on a monolayer of LSECs, stained by F4/80 antibody and the number of F4/80-positive cells was counted (Fig. 6H and I). AEG-1$^{-/-}$ Kupffer cells showed significant reduction in adhesion ability compared with AEG-1$^{+/+}$ Kupffer cells further establishing functional inactivation of AEG-1$^{-/-}$ macrophages.

Discussion

Exploiting a conditional knockout mouse system we document, for the first time, the inherent necessity for AEG-1 in macrophage activation. The functional anergy of the Kupffer cells and BMDMs is similar to what is observed in normal small intestinal macrophages. The human small intestinal mucosa is characterized by resistance to inflammation, even though there is constant exposure to bacterial products, because of an inherent anergy of intestinal macrophages, which fail to respond to TLR ligands and have marked inability to activate MyD88-dependent and -independent NFκB signaling pathway (42). In the absence of AEG-1, Kupffer cells and BMDMs are unable to activate NFκB

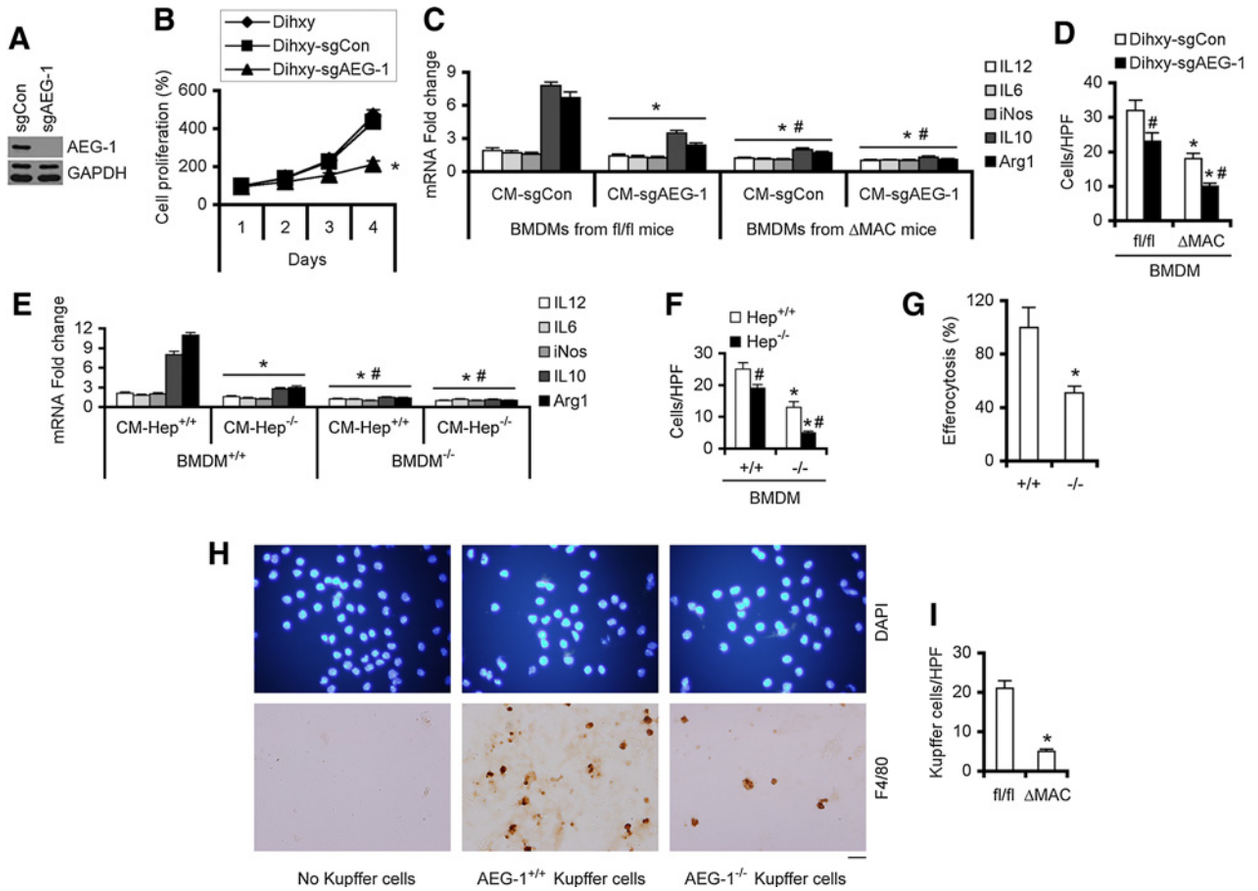

Figure 6.

AEG-1$^{-/-}$ macrophages show functional anergy. **A,** Western blot analysis for AEG-1 in Dihxy-sgCon (sgCon) and Dihxy-sgAEG-1 (sgAEG-1) cells. **B,** Cell proliferation by MTT assay in the indicated clones. Data represent mean ± SEM of triplicate experiments, each containing eight data points per group. *, $P < 0.01$ versus Dihxy and Dihxy-sgCon. **C,** AEG-1$^{+/+}$ and AEG-1$^{-/-}$ BMDMs, isolated from AEG-1$^{fl/fl}$ and AEG-1$^{\Delta MAC}$ mice, respectively, were treated with CM from Dihxy-sgCon and Dihxy-sgAEG-1 cells and the levels of the indicated mRNAs were measured by TaqMan qRT-PCR. Data represent mRNA fold change over untreated samples and were normalized by GAPDH levels. Data represent mean ± SEM of triplicate experiments. *, $P < 0.01$ versus BMDMs isolated from AEG-1$^{fl/fl}$ mice treated with CM-sgCon; #, $P < 0.01$ versus BMDMs isolated from AEG-1$^{fl/fl}$ mice treated with CM-sgAEG-1. **D,** Migration of AEG-1$^{+/+}$ and AEG-1$^{-/-}$ BMDMs, isolated from AEG-1$^{fl/fl}$ and AEG-1$^{\Delta MAC}$ mice, respectively, toward Dihxy-sgCon and Dihxy-sgAEG-1 cells. Data represent mean ± SEM of triplicate experiments. *, $P < 0.01$ versus corresponding AEG-1$^{+/+}$; #, $P < 0.01$ versus corresponding Dihxy-sgCon. **E** and **F,** AEG-1$^{+/+}$ and total AEG-1$^{-/-}$ mice were injected with DEN (10 μg/g) at 2 weeks and transformed hepatocytes and BMDMs were isolated at 12 weeks. AEG-1$^{+/+}$ and AEG-1$^{-/-}$ BMDMs were treated with CM from AEG-1$^{+/+}$ and AEG-1$^{-/-}$ hepatocytes and the levels of the indicated mRNAs were measured by TaqMan qRT-PCR (**E**). Data represent mRNA fold change over untreated samples and were normalized by GAPDH levels. Data represent mean ± SEM of triplicate experiments. *, $P < 0.01$ versus BMDMs$^{+/+}$ treated with CM-Hep$^{+/+}$; #, $P < 0.01$ versus BMDM$^{+/+}$ treated with CM-Hep$^{-/-}$. **F**, Migration of AEG-1$^{+/+}$ and AEG-1$^{-/-}$ BMDMs toward AEG-1$^{+/+}$ and AEG-1$^{-/-}$ hepatocytes. Data represent mean ± SEM of triplicate experiments. *, $P < 0.01$ versus corresponding AEG-1$^{+/+}$ BMDMs; #, $P < 0.01$ versus corresponding AEG-1$^{+/+}$ hepatocytes. **G,** Efferocytosis of AEG-1$^{+/+}$ and AEG-1$^{-/-}$ peritoneal macrophages. Data represent mean ± SEM of triplicate experiments. *, $P < 0.01$. **H,** Representative images of adherent AEG-1$^{+/+}$ and AEG-1$^{-/-}$ Kupffer cells, isolated from AEG-1$^{fl/fl}$ and AEG-1$^{\Delta MAC}$ mice, to LSECs. Magnification, ×400. Scale bar, 20 μm. **I,** Quantification of adherent AEG-1$^{+/+}$ and AEG-1$^{-/-}$ Kupffer cells to LSECs per high power field (HPF). Data represent mean ± SEM of triplicate experiments. *, $P < 0.01$ versus AEG-1$^{+/+}$.

signaling and show severe anergy so that they do not respond to any external stimuli and become functionally inactive. The basal expression of AEG-1 in human small intestine is markedly lower than that in the liver (43), suggesting that it might be the decreased level of AEG-1 that renders small intestinal macrophages anergic.

Induction of senescence in premalignant cells is a mechanism of HCC inhibition (37). We previously documented that Alb/AEG-1 hepatocytes show robust resistance to induction of senescence, which is accompanied by dampening of induction of a DNA damage response compared with wild-type hepatocytes over a period of 7 days of *in vitro* culture (18). DEN strongly activates DNA damage signaling in hepatocytes, resulting in the activation of p53 (44). We now document that *in vitro* culture–induced senescence and DEN-induced DNA damage response are augmented in AEG-1$^{-/-}$ hepatocytes. AEG-1$^{-/-}$ hepatocytes are also more sensitive to DEN-induced cell death compared with wild-type. In addition, AEG-1$^{-/-}$ hepatocytes display a profound sensitivity to a wide variety of stressors. These findings indicate that in the absence of AEG-1, hepatocytes may not overcome apoptosis, such as those induced by DEN, so that all DEN-

damaged hepatocytes die off precluding escape and survival of mutated, transformed hepatocytes. The presence of AEG-1 allows wild-type hepatocytes to overcome DEN-induced stress, and overexpression of AEG-1 facilitates the transformed cells ability to overcome a variety of stresses, such as hypoxia and nutrient deprivation, brought forth by the tumorigenic process. The response of AEG-$1^{\Delta HEP}$ mice to DEN is similar to that of ATM-deficient mice in which robust activation of DEN-induced ATR-Chk1-p53 renders them resistant to DEN-induced HCC (44).

Studies in mouse models have established a pivotal role of NFκB in regulating HCC development and progression. However, the regulatory role of NFκB is context dependent. $Mdr2^{-/-}$ mice develop spontaneous cholestatic hepatitis and HCC (10, 45). Overexpression of a nondegradable mutant IκBα that blocks NFκB activation significantly inhibited HCC progression in this model (10). Hepatocyte-specific knockout of IKKβ abrogated HCC development in a transgenic mouse overexpressing lymphotoxinα and/or β (46). On the contrary, hepatocyte-specific knockout of IKKβ promoted HCC development in DEN-initiation model and hepatocyte-specific knockout of IKKγ resulted in spontaneous development of HCC (5, 47). ROS-induced JNK and STAT3 activation has been suggested to promote HCC in IKKβ knockout model and IKKβ has been suggested to inhibit both hepatic injury and proliferation (7). However, deletion of IKKβ in macrophages significantly abrogated DEN-induced HCC (5). In addition, genetic deletion of IL6 or inhibition of inflammatory cytokines, such as TNFα, provided a significant reduction in tumor load (8). In addition to activating NFκB, AEG-1 activates a plethora of oncogenic signaling pathways and modulates gene expression at transcriptional, posttranscriptional, and translational levels in tumor cells (48). As such, the phenotypes observed in AEG-$1^{\Delta HEP}$ mice are not corollary to hepatocyte-specific IKKβ–knockout mice. On the contrary, phenotypes of AEG-$1^{\Delta MAC}$ mice are similar to macrophage-specific IKKβ knockout mice, further confirming a fundamental requirement of NFκB in macrophage activation.

The current studies indicate that targeting AEG-1 in both hepatocytes and macrophages might be an effective way in combating HCC. We recently demonstrated that hepatocyte-targeted nanoparticles delivering AEG-1 siRNA profoundly inhibited growth of orthotopic xenografts of human HCC cells in nude mice (49). In the scenario of endogenous HCC, both hepatocyte- and macrophage-targeted nanoparticles delivering AEG-1 siRNA might exert a more robust and sustained anti-HCC effect. Studies are in progress to evaluate this hypothesis.

Disclosure of Potential Conflicts of Interest

No potential conflicts of interest were disclosed.

Authors' Contributions

Conception and design: C.L. Robertson, D. Sarkar
Development of methodology: C.L. Robertson, N.D. Mukhopadhyay, M.A. Subler, S. Ghosh, D. Sarkar
Acquisition of data (provided animals, acquired and managed patients, provided facilities, etc.): C.L. Robertson, R.G. Mendoza, N. Jariwala, M.A. Subler, J.J. Windle, Z. Lai, S. Ghosh, D. Sarkar
Analysis and interpretation of data (e.g., statistical analysis, biostatistics, computational analysis): C.L. Robertson, M. Dozmorov, N.D. Mukhopadhyay, D. Sarkar
Writing, review, and/or revision of the manuscript: C.L. Robertson, M. Dozmorov, N.D. Mukhopadhyay, P.B. Fisher, S. Ghosh, D. Sarkar
Administrative, technical, or material support (i.e., reporting or organizing data, constructing databases): C.L. Robertson, R.G. Mendoza, D. Sarkar
Study supervision: D. Sarkar

Acknowledgments

D. Sarkar is the Harrison Foundation Distinguished Professor in Cancer Research. P.B. Fisher holds the Thelma Newmeyer Corman Chair in Cancer Research. This study was supported in part by The National Institute of Diabetes and Digestive and Kidney Diseases (NIDDK) grant 1R01DK107451-01A1 (to D. Sarkar) and a Virginia Commonwealth University Massey Cancer Center pilot project grant (to D. Sarkar and S. Ghosh). Services in support of this project were provided by the VCU Massey Cancer Center Transgenic/Knock-out Mouse Facility and flow cytometry core facility, supported in part with funding from NIH/NCI Cancer Center Support Grant P30 CA016059.

The costs of publication of this article were defrayed in part by the payment of page charges. This article must therefore be hereby marked *advertisement* in accordance with 18 U.S.C. Section 1734 solely to indicate this fact.

Received March 1, 2018; revised July 25, 2018; accepted August 28, 2018; published first September 4, 2018.

Reference

1. El-Serag HB. Hepatocellular carcinoma. N Engl J Med 2011;365:1118–27.
2. Krenkel O, Tacke F. Liver macrophages in tissue homeostasis and disease. Nat Rev Immunol 2017;17:306–21.
3. Sakurai T, He G, Matsuzawa A, Yu GY, Maeda S, Hardiman G, et al. Hepatocyte necrosis induced by oxidative stress and IL-1 alpha release mediate carcinogen-induced compensatory proliferation and liver tumorigenesis. Cancer Cell 2008;14:156–65.
4. Naugler WE, Sakurai T, Kim S, Maeda S, Kim K, Elsharkawy AM, et al. Gender disparity in liver cancer due to sex differences in MyD88-dependent IL-6 production. Science 2007;317:121–4.
5. Maeda S, Kamata H, Luo JL, Leffert H, Karin M. IKKbeta couples hepatocyte death to cytokine-driven compensatory proliferation that promotes chemical hepatocarcinogenesis. Cell 2005;121:977–90.
6. He G, Dhar D, Nakagawa H, Font-Burgada J, Ogata H, Jiang Y, et al. Identification of liver cancer progenitors whose malignant progression depends on autocrine IL-6 signaling. Cell 2013;155:384–96.
7. He G, Yu GY, Temkin V, Ogata H, Kuntzen C, Sakurai T, et al. Hepatocyte IKKbeta/NF-kappaB inhibits tumor promotion and progression by preventing oxidative stress-driven STAT3 activation. Cancer Cell 2010;17:286–97.
8. Park EJ, Lee JH, Yu GY, He G, Ali SR, Holzer RG, et al. Dietary and genetic obesity promote liver inflammation and tumorigenesis by enhancing IL-6 and TNF expression. Cell 2010;140:197–208.
9. Lanaya H, Natarajan A, Komposch K, Li L, Amberg N, Chen L, et al. EGFR has a tumour-promoting role in liver macrophages during hepatocellular carcinoma formation. Nat Cell Biol 2014;16:972–7.
10. Pikarsky E, Porat RM, Stein I, Abramovitch R, Amit S, Kasem S, et al. NF-kappaB functions as a tumour promoter in inflammation-associated cancer. Nature 2004;431:461–6.
11. Wan S, Kuo N, Kryczek I, Zou W, Welling TH. Myeloid cells in hepatocellular carcinoma. Hepatology 2015;62:1304–12.
12. Yoo BK, Emdad L, Su ZZ, Villanueva A, Chiang DY, Mukhopadhyay ND, et al. Astrocyte elevated gene-1 regulates hepatocellular carcinoma development and progression. J Clin Invest 2009;119:465–77.
13. Yoo BK, Chen D, Su Z-Z, Gredler R, Yoo J, Shah K, et al. Molecular mechanism of chemoresistance by astrocyte elevated gene-1 (AEG-1). Cancer Res 2010;70:3249–58.
14. Yoo BK, Gredler R, Vozhilla N, Su ZZ, Chen D, Forcier T, et al. Identification of genes conferring resistance to 5-fluorouracil. Proc Natl Acad Sci U S A 2009;106:12938–43.

15. Yoo BK, Santhekadur PK, Gredler R, Chen D, Emdad L, Bhutia SK, et al. Increased RNA-induced silencing complex (RISC) activity contributes to hepatocelllular carcinoma. Hepatology 2011;53:1538–48.
16. Srivastava J, Robertson CL, Gredler R, Siddiq A, Rajasekaran D, Akiel MA, et al. Astrocyte elevated gene-1 (AEG-1) contributes to non-thyroidal illness syndrome (NTIS) associated with hepatocellular carcinoma (HCC). J Biol Chem 2015;290:15549–58.
17. Srivastava J, Robertson CL, Rajasekaran D, Gredler R, Siddiq A, Emdad L, et al. AEG-1 regulates retinoid X receptor and inhibits retinoid signaling. Cancer Res 2014;74:4364–77.
18. Srivastava J, Siddiq A, Emdad L, Santhekadur P, Chen D, Gredler R, et al. Astrocyte elevated gene-1 (AEG-1) promotes hepatocarcinogenesis: novel insights from a mouse model. Hepatology 2012;56:1782–91.
19. Srivastava J, Siddiq A, Gredler R, Shen XN, Rajasekaran D, Robertson CL, et al. Astrocyte elevated gene-1 and c-Myc cooperate to promote hepatocarcinogenesis in mice. Hepatology 2015;61:915–29.
20. Robertson CL, Srivastava J, Siddiq A, Gredler R, Emdad L, Rajasekaran D, et al. Genetic deletion of AEG-1 prevents hepatocarcinogenesis. Cancer Res 2014;74:6184–93.
21. Gong Z, Liu W, You N, Wang T, Wang X, Lu P, et al. Prognostic significance of metadherin overexpression in hepatitis B virus-related hepatocellular carcinoma. Oncol Rep 2012;27:2073–9.
22. Srivastava J, Robertson CL, Ebeid K, Dozmorov M, Rajasekaran D, Mendoza R, et al. A novel role of astrocyte elevated gene-1 (AEG-1) in regulating nonalcoholic steatohepatitis (NASH). Hepatology 2017;66:466–80.
23. Emdad L, Sarkar D, Su ZZ, Randolph A, Boukerche H, Valerie K, et al. Activation of the nuclear factor kappaB pathway by astrocyte elevated gene-1: implications for tumor progression and metastasis. Cancer Res 2006;66:1509–16.
24. Sarkar D, Park ES, Emdad L, Lee SG, Su ZZ. Fisher Molecular basis of nuclear factor-kappaB activation by astrocyte elevated gene-1. Cancer Res 2008; 68:1478–84.
25. Alexia C, Poalas K, Carvalho G, Zemirli N, Dwyer J, Dubois SM, et al. The endoplasmic reticulum acts as a platform for ubiquitylated components of nuclear factor kappaB signaling. Sci Signal 2013;6:ra79.
26. Krishnan RK, Nolte H, Sun T, Kaur H, Sreenivasan K, Looso M, et al. Quantitative analysis of the TNF-alpha-induced phosphoproteome reveals AEG-1/MTDH/LYRIC as an IKKbeta substrate. Nat Comm 2015;6:6658.
27. Vartak-Sharma N, Gelman BB, Joshi C, Borgamann K, Ghorpade A. Astrocyte elevated gene-1 is a novel modulator of HIV-1-associated neuroinflammation via regulation of nuclear factor-kappaB signaling and excitatory amino acid transporter-2 repression. J Biol Chem 2014;289: 19599–612.
28. Vartak-Sharma N, Ghorpade A. Astrocyte elevated gene-1 regulates astrocyte responses to neural injury: implications for reactive astrogliosis and neurodegeneration. J Neuroinflam 2012;9:195.
29. Yakar S, Liu JL, Stannard B, Butler A, Accili D, Sauer B, et al. Normal growth and development in the absence of hepatic insulin-like growth factor I. Proc Natl Acad Sci U S A 1999;96:7324–9.
30. Clausen BE, Burkhardt C, Reith W, Renkawitz R, Forster I. Conditional gene targeting in macrophages and granulocytes using LysMcre mice. Transgenic Res 1999;8:265–77.
31. Bissell DM, Guzelian PS. Phenotypic stability of adult rat hepatocytes in primary monolayer culture. Ann NY Acad Sci 1980;349:85–98.
32. Bissell DM, Guzelian PS. Degradation of endogenous hepatic heme by pathways not yielding carbon monoxide. Studies in normal rat liver and in primary hepatocyte culture. J Clin Invest 1980;65:1135–40.
33. Zhang X, Goncalves R, Mosser DM. The isolation and characterization of murine macrophages. Curr Protoc Immunol 2008;Chapter 14:Unit 14 1.
34. Meyer J, Lacotte S, Morel P, Gonelle-Gispert C, Buhler L. An optimized method for mouse liver sinusoidal endothelial cell isolation. Exp Cell Res 2016;349:291–301.
35. Chen D, Yoo BK, Santhekadur PK, Gredler R, Bhutia SK, Das SK, et al. Insulin-like growth factor-binding protein-7 functions as a potential tumor suppressor in hepatocellular carcinoma. Clin Cancer Res 2011;17: 6693–701.
36. Verna L, Whysner J, Williams GM. N-nitrosodiethylamine mechanistic data and risk assessment: bioactivation, DNA-adduct formation, mutagenicity, and tumor initiation. Pharmacol Ther 1996;71:57–81.
37. Kang TW, Yevsa T, Woller N, Hoenicke L, Wuestefeld T, Dauch D, et al. Senescence surveillance of pre-malignant hepatocytes limits liver cancer development. Nature 2011;479:547–51.
38. Qian BZ, Pollard JW. Macrophage diversity enhances tumor progression and metastasis. Cell 2010;141:39–51.
39. Mantovani A, Allavena P, Sica A. Tumour-associated macrophages as a prototypic type II polarised phagocyte population: role in tumour progression. Eur J Cancer 2004;40:1660–7.
40. Lewis CE, Pollard JW. Distinct role of macrophages in different tumor microenvironments. Cancer Res 2006;66:605–12.
41. Moore KJ, Tabas I. Macrophages in the pathogenesis of atherosclerosis. Cell 2011;145:341–55.
42. Smythies LE, Shen R, Bimczok D, Novak L, Clements RH, Eckhoff DE, et al. Inflammation anergy in human intestinal macrophages is due to Smad-induced IkappaBalpha expression and NF-kappaB inactivation. J Biol Chem 2010;285:19593–604.
43. Kang DC, Su ZZ, Sarkar D, Emdad L, Volsky DJ, Fisher PB. Cloning and characterization of HIV-1-inducible astrocyte elevated gene-1, AEG-1. Gene 2005;353:8–15.
44. Teoh N, Pyakurel P, Dan YY, Swisshelm K, Hou J, Mitchell C, et al. Induction of p53 renders ATM-deficient mice refractory to hepatocarcinogenesis. Gastroenterology 2010;138:1155–65.
45. Mauad TH, van Nieuwkerk CM, Dingemans KP, Smit JJ, Schinkel AH, Notenboom RG, et al. Mice with homozygous disruption of the mdr2 P-glycoprotein gene. A novel animal model for studies of nonsuppurative inflammatory cholangitis and hepatocarcinogenesis. Am J Pathol 1994; 145:1237–45.
46. Haybaeck J, Zeller N, Wolf MJ, Weber A, Wagner U, Kurrer MO, et al. A lymphotoxin-driven pathway to hepatocellular carcinoma. Cancer Cell 2009;16:295–308.
47. Luedde T, Beraza N, Kotsikoris V, van Loo G, Nenci A, De Vos R, et al. Deletion of NEMO/IKKgamma in liver parenchymal cells causes steatohepatitis and hepatocellular carcinoma. Cancer Cell 2007;11:119–32.
48. Sarkar D, Fisher PB. AEG-1/MTDH/LYRIC: clinical significance. Adv Cancer Res 2013;120:39–74.
49. Rajasekaran D, Srivastava J, Ebeid K, Gredler R, Akiel M, Jariwala N, et al. Combination of nanoparticle-delivered siRNA for Astrocyte elevated gene-1 (AEG-1) and all-trans retinoic acid (ATRA): an effective therapeutic strategy for hepatocellular carcinoma (HCC). Bioconjug Chem 2015;26: 1651–61.